https://dx.doi.org/10.1016/j.ymssp.2020.106965

To: Mechanical Systems and Signal Processing

Sparse Bayesian learning for structural damage detection under varying temperature conditions

Rongrong Hou
Department of Civil and Environmental Engineering,
The Hong Kong Polytechnic University,
Kowloon, Hong Kong, P. R. China
rongrong.hou@connect.polyu.hk

Xiaoyou Wang
Department of Civil and Environmental Engineering,
The Hong Kong Polytechnic University,
Kowloon, Hong Kong, P. R. China
xiaoyou.wang@connect.polyu.hk

Qi Xia
Department of Civil and Environmental Engineering,
The Hong Kong Polytechnic University,
Kowloon, Hong Kong, P. R. China
q.xia@polyu.edu.hk

Yong Xia*
Professor,
Department of Civil and Environmental Engineering,
The Hong Kong Polytechnic University,
Kowloon, Hong Kong, P. R. China
ceyxia@polyu.edu.hk

(*Corresponding author)

Abstract

Structural damage detection inevitably entails uncertainties, such as measurement noise and modelling errors. The existence of uncertainties may cause incorrect damage detection results. In addition, varying environmental conditions, especially temperature, may have a more significant effect on structural responses than structural damage does. Neglecting the temperature effects may make reliable damage detection difficult. In this study, a new vibration based damage detection technique that simultaneously considers the uncertainties and varying temperature conditions is developed in the sparse Bayesian learning framework. The structural vibration properties are treated as the function of both the damage parameter and varying temperature. The temperature effects on the vibration properties are incorporated into the Bayesian model updating on the basis of the quantitative relation between temperature and natural frequencies. The structural damage parameter and associated hyper-parameters are then solved through the iterative expectation–maximization technique. An experimental frame is utilized to demonstrate the effectiveness of the proposed damage detection method. The sparse damage is located and quantified correctly by considering the varying temperature conditions.

Keywords

Structural damage detection, sparse Bayesian learning, uncertainty, temperature effects, expectation–maximization

1. Introduction

Over the last decades, numerous vibration-based damage identification methods have been developed [1-5]. Amongst various vibration properties, frequencies [6, 7] and mode shapes [8, 9] are most widely used for damage detection. The fast development in sensing technologies [10], signal processing techniques [11] and machine learning [12], has advanced vibration-based damage identification methods over the past decade. Huang et al. [13] presented a complete review of the recent development of Bayesian inference for structural damage detection and assessment. Gordan et al. [14] intensively reviewed the applications of data mining techniques in damage identification and structural health monitoring (SHM) since 2000. Bao et al. [15] reviewed advancements in data science and engineering in SHM.

The vibration-based damage detection is essentially an inverse problem and typically ill-posed. Furthermore, such detection is usually an underdetermined problem in mathematics because the number of available vibration measurements is limited. In practice, structural damage commonly appears in a few sections or members only. Thus, damage is spatially sparse compared with the numerous elements of the entire structure. In recent years, some researchers have developed the sparse recovery theory for structural damage identification by using the so-called l_1 and l_0 regularisation techniques [16-21]. However, this sparse recovery theory disregards the relative uncertainties between different variables and causes difficulties in the determination of the regularisation parameter. Moreover, the relationship between the resulting unique solution and that of the original unregularised problem is uncertain [22].

Another difficulty in structural damage detection is that civil structures are generally subject to significant uncertainties including measurement noise and modelling errors, which may lead to incorrect damage identification [23, 24]. For example, the existence of measurement noise may mask subtle changes in the vibration properties caused by damage. Therefore, deterministic methods may fail when applied to real civil structures.

In recent decades, many statistical damage identification techniques have been developed and

the uncertainties are considered as random variables [25]. The representative techniques include perturbation methods [23], Monte Carlo simulation [26], statistical pattern recognition [27] and Bayesian methods [28-31]. Amongst them, the Bayesian methods have attracted considerable attention since the 1990s. Apart from addressing uncertainties, the Bayesian methods also provide an efficient way to deal with the ill-posed inverse problem by specifying probability distributions over the uncertain parameters, which is equivalent to introducing a regularisation term to the optimisation problem [32].

For civil engineering structures, additional practical challenge is that the structural vibration properties may vary under the operational and environmental conditions, particularly temperature. Temperature variation may change the material properties [33, 34] and boundary conditions [35-37] of a structure and thus alter the structural modal parameters [38, 39]. Many field studies have been conducted to investigate the effect of temperature on the structural modal properties since the 1970s [40-42]. Some studies modelled and quantified the temperature effects on natural frequencies based on the Bayesian probabilistic framework [43]. Previous studies demonstrated that varying temperature may cause more significant changes in the structural vibration properties than damage does [38, 40, 44]. Consequently, if the temperature effects are not considered appropriately, then reliable damage detection becomes difficult. Researchers [45-51] have developed various techniques to consider the effects of temperature on damage identification. These approaches can be divided into two categories depending on whether the environmental variables are measured or not. However, few has studied the uncertainties and varying temperature simultaneously.

In this study, a new probabilistic damage detection technique considering both uncertainties and varying temperature is developed on the basis of sparse Bayesian learning (SBL). The quantitative relation between temperature and structural modal parameters is incorporated into the Bayesian model updating framework. The expectation–maximization (EM) technique is employed to calculate the structural damage parameter and hyper-parameters in an iterative manner. An experimental example demonstrates that the damage identification results are more accurate than those without considering the varying temperature conditions.

2. SBL Modelling Considering Varying Temperature

The Bayesian approach provides a rigorous probabilistic framework, in which the posterior probability of the uncertain quantities is explicitly quantified according to prior information and current measurement data. The posterior probability distribution of the unknown parameter θ given the measurement data $\boldsymbol{\mathcal{D}}$ and chosen class of models $\mathcal{M}$, can be expressed as [30]

$$p(\boldsymbol{\theta}|\boldsymbol{\mathcal{D}},\mathcal{M}) = c^{-1}p(\boldsymbol{\mathcal{D}}|\boldsymbol{\theta},\mathcal{M})p(\boldsymbol{\theta}|\mathcal{M}) \quad (1)$$

where $p(\boldsymbol{\mathcal{D}}|\boldsymbol{\theta},\mathcal{M})$ is the likelihood function and can be interpreted as a measure of the plausibility of the measurement data $\boldsymbol{\mathcal{D}}$ according to the model parameterised by $\boldsymbol{\theta}$, $p(\boldsymbol{\theta}|\mathcal{M})$ is the prior probability density function (PDF), and $\mathrm{c} = p(\boldsymbol{\mathcal{D}}|\,\mathcal{M})$ is the normalizing constant that is referred to as the evidence.

2.1 Measurement data

Suppose that N_m modes of vibration properties of a structure have been measured and the natural frequencies and mode shapes are as

$$\hat{\boldsymbol{\lambda}} = [\hat{\lambda}_1, \hat{\lambda}_2, \cdots, \hat{\lambda}_{N_m}] \quad (2)$$

$$\hat{\boldsymbol{\Psi}} = [\hat{\boldsymbol{\phi}}_1, \hat{\boldsymbol{\phi}}_2, \cdots, \hat{\boldsymbol{\phi}}_{N_m}] \quad (3)$$

where λ_r is the rth natural frequency and $\hat{\boldsymbol{\phi}}_r \in \mathbb{R}^{N_p}$ denotes the identified rth mode shape at N_p measurement points. The modal data including the natural frequencies and mode shapes in the nth test are expressed as $\hat{\Upsilon}_n$. The modal and temperature data from N_s tests are denoted as $\boldsymbol{\mathcal{D}}_Y = \{\hat{\Upsilon}_1, \ldots, \hat{\Upsilon}_{N_s}\}$ and $\boldsymbol{\mathcal{D}}_T = \{\hat{T}_1, \ldots, \hat{T}_{N_s}\}$, respectively.

2.2 Structural model class

The structural model class, $\mathcal{M}$, is based on a set of linear structural models parameterised by the model parameters $\mathbf{s} \in \mathbb{R}^N$. The rth natural frequency and the corresponding mode shape

are governed by the following eigenvalue equation

$$\mathbf{K}(\mathbf{s})\boldsymbol{\phi}_r = \lambda_r^2 \mathbf{M}\boldsymbol{\phi}_r \tag{4}$$

where $\mathbf{M}$ is a known mass matrix and $\mathbf{K}$ is an uncertain stiffness matrix parameterised as follows

$$\mathbf{K}(\mathbf{s}) = \sum_{i=1}^{N_e} s_i \mathbf{K}_i \tag{5}$$

where $\mathbf{K}_i$ is the *i*th element stiffness matrix, which can be obtained through finite element (FE) analysis of the structure, s_i is the *i*th element stiffness parameter to be updated according to the observations, and N_e is the number of structural elements.

The change in the mass is assumed to be negligible when damage occurs. Therefore, the structural stiffness matrix in the damaged state takes the following form [19]

$$\bar{\mathbf{K}}(\mathbf{s}) = \sum_{i=1}^{N} \bar{s}_i \mathbf{K}_i \tag{6}$$

where $\bar{s}_i$ is the *i*th element stiffness parameter in the damaged state. The stiffness reduction factor (SRF), defined as the damage parameter, is calculated as

$$\theta_i = \frac{\bar{s}_i - s_i}{s_i} \tag{7}$$

The values of SRF indicate both damage location and damage severity. Since structural damage usually occurs in a few sections or members only, $\boldsymbol{\theta} \in \mathbb{R}^N$ is a sparse vector with several non-zero items at the damaged locations and zeros at most of others.

2.3 Likelihood function for structural damage parameters and temperatures

To consider the continuous accumulation of data, the probabilistic distribution of the model prediction of the current data is assumed unaffected by the previous predicted ones. Hence the likelihood function is constructed as

$$p(\boldsymbol{\mathcal{D}}_Y|\boldsymbol{\theta}) = \prod_{n=1}^{N_s} p\left(\hat{\Upsilon}_n|\boldsymbol{\theta}\right) \tag{8}$$

Given the structural damage parameter $\boldsymbol{\theta}$, the new measurement data can be incorporated into the likelihood function in a systematic and continuous manner by simply augmenting the

product with one term [30]. Consequently, the probability of damage for each element or substructure can be continuously updated, which well fulfils the requirement of online structural health monitoring.

In the present study, temperature is treated as a variable of the modal data. Consequently, the modal data are a function of both the structural damage parameter and temperature. Eq. (8) is thus expanded to include temperature as

$$p(\boldsymbol{\mathcal{D}}_Y, \boldsymbol{\mathcal{D}}_T|\boldsymbol{\theta}, \boldsymbol{T}) = \prod_{n=1}^{N_S} p\left(\hat{\Upsilon}_n, \hat{T}_n|\boldsymbol{\theta}, T_n\right) \tag{9}$$

The modal data are assumed independent mode by mode. It has

$$p(\boldsymbol{\mathcal{D}}_Y, \boldsymbol{\mathcal{D}}_T|\boldsymbol{\theta}, \boldsymbol{T}) = \prod_{n=1}^{N_S}\prod_{r=1}^{N_m} p\left(\hat{\lambda}_{r,n}|\boldsymbol{\theta}, T_n\right) \prod_{r=1}^{N_m} p\left(\hat{\boldsymbol{\phi}}_{\boldsymbol{r}}|\boldsymbol{\theta}\right) \prod_{n=1}^{N_S} p\left(\hat{T}_n|T_n\right) \tag{10}$$

Most previous studies have demonstrated that natural frequencies of a structure decrease with an increase in temperature. This decrease is due to that the increase in temperature will cause the decrease in the Young's modulus and shear modulus for most construction materials [33, 38]. Moreover, it has been widely accepted that the effect of temperature on mode shapes is negligible [38, 52]. Therefore, the temperature influence on the natural frequencies should be characterised prior to conducting damage identification. Most studies have demonstrated that the natural frequencies have a linear relation with temperature [38, 53]. In this regard, the natural frequency is expressed as

$$\hat{\lambda}_r(\boldsymbol{\theta}, T)\left(1 + \varepsilon_{\lambda_r}\right) = \lambda_r(\boldsymbol{\theta}, T_0) + \Delta\lambda_r(\boldsymbol{\theta}, \Delta T) = \lambda_r(\boldsymbol{\theta}, T_0) + b_r(T - T_0) \tag{11}$$

$$\varepsilon_{\lambda_r} \sim N(0, \beta^{-1}) \tag{12}$$

where $\lambda_r(\boldsymbol{\theta}, T_0)$ is the rth natural frequency at a reference temperature T_0, $\Delta\lambda_r(\boldsymbol{\theta}, \Delta T)$ is the frequency change caused by the temperature variation $\Delta T = T - T_0$, and b_r is the coefficient for the rth natural frequency. The hyper-parameter β, which is equal to the reciprocal of the variance of the variable, reflects the precision of the identified natural frequency. To simplify the notation, the dependence of the natural frequency on the temperature is dropped hereafter, expressed as $\lambda_r(\boldsymbol{\theta})$.

The measured mode shape is expressed as

$$\boldsymbol{\phi}_r(\boldsymbol{\theta}) = \hat{\boldsymbol{\phi}}_r + \boldsymbol{\varepsilon}_{\boldsymbol{\phi}_r} \tag{13}$$

$$\boldsymbol{\varepsilon}_{\boldsymbol{\phi}_r} \sim N(0,\ \gamma^{-1}\boldsymbol{I}) \tag{14}$$

The measurement error of temperature is also considered and modelled as a Gaussian random variable, that is,

$$T = \hat{T} + \varepsilon_T \tag{15}$$

$$\varepsilon_T \sim N(0,\ \rho^{-1}) \tag{16}$$

where hyper-parameters γ and ρ reflect the precision of the measured mode shapes $\hat{\boldsymbol{\phi}}$ and temperature $\hat{T}$, respectively.

The resulting likelihood functions of $\boldsymbol{\theta}$ and $\boldsymbol{T}$ based on $\boldsymbol{\mathcal{D}}_Y$ and $\boldsymbol{\mathcal{D}}_T$ are expressed as

$$p\left(\hat{\boldsymbol{\lambda}}\middle|\boldsymbol{\theta},\boldsymbol{T},\beta,\boldsymbol{b}\right) = \left(\frac{\beta}{2\pi}\right)^{\frac{N_m \cdot N_s}{2}} exp\left\{-\frac{\beta}{2}\sum_{n=1}^{N_s}\sum_{r=1}^{N_m}\left[\frac{\lambda_{r,n}(\boldsymbol{\theta}) + b_r(T_n - T_0) - \hat{\lambda}_{r,n}}{\hat{\lambda}_{r,n}}\right]^2\right\} \tag{17}$$

$$p\left(\hat{\boldsymbol{\phi}}\middle|\boldsymbol{\theta},\gamma\right) = \left(\frac{\gamma}{2\pi}\right)^{\frac{N_p \cdot N_m}{2}} exp\left\{-\frac{\gamma}{2}\sum_{r=1}^{N_m}\sum_{j=1}^{N_p}\left[\hat{\phi}_{j,r} - \phi_{j,r}(\boldsymbol{\theta})\right]^2\right\} \tag{18}$$

$$p\left(\hat{\boldsymbol{T}}\middle|\boldsymbol{T},\rho\right) = \left(\frac{\rho}{2\pi}\right)^{\frac{N_s}{2}} exp\left\{-\frac{\rho}{2}\sum_{n=1}^{N_s}\left(\hat{T}_n - T_n\right)^2\right\} \tag{19}$$

where $\hat{\lambda}_{r,n}$ denotes the *r*th identified natural frequency under temperature $\hat{T}_n$.

2.4 Prior distribution of damage parameter

In the Bayesian framework, the prior distribution is independent of current measurement and is chosen on the basis of engineering and modelling judgement. As introduced previously, the structural damage parameter $\boldsymbol{\theta}$ is a sparse vector with a few non-zero items at the damaged locations and many zeros at the others. According to the SBL framework, the automatic relevance determination (ARD) prior is adopted to promote sparsity in the damage parameter [54-56]. The damage parameter $\boldsymbol{\theta}$ is assumed to be in Gaussian distribution and an

individual hyper-parameter is assigned to each damage parameter, namely,

$$p(\boldsymbol{\theta}|\boldsymbol{\alpha}) = \prod_{i=1}^{N_e} p(\theta_i|\alpha_i) = \left(\frac{1}{2\pi}\right)^{\frac{N_e}{2}} \prod_{i=1}^{N_e} \left[\alpha_i^{\frac{1}{2}} exp\left\{-\frac{1}{2}\alpha_i\theta_i^2\right\}\right] \tag{20}$$

where the hyper-parameter α_i represents the precision of θ_i. The ARD prior closely resembles the l_0 regularization introduced to the ill-posed inverse damage detection problem [57, 58]. Recently, some researchers studied the prediction-error variance model. To analyse the general heterogeneous cases, Mu and Yuen (2016) relaxed the homogeneity assumption on the errors by embedding the derived closed-form expression of the error variance parameter optimization component into the hyper-parameter optimization of ARD prior [59].

2.5 Posterior distribution for damage parameter and temperature

According to Eqs. (1) and (10), the joint posterior PDF of the damage parameter $\boldsymbol{\theta}$ and temperature $\boldsymbol{T}$ is then calculated as

$$p\left(\boldsymbol{\theta}, \boldsymbol{T}|\hat{\boldsymbol{\lambda}}, \hat{\boldsymbol{\psi}}, \hat{\boldsymbol{T}}, \beta, \boldsymbol{b}, \gamma, \rho, \boldsymbol{\alpha}\right) \propto p\left(\hat{\boldsymbol{\lambda}}|\boldsymbol{\theta}, \boldsymbol{T}, \beta, \boldsymbol{b}\right) p\left(\hat{\boldsymbol{\psi}}|\boldsymbol{\theta}, \gamma\right) p\left(\hat{\boldsymbol{T}}|\boldsymbol{T}, \rho\right) p(\boldsymbol{\theta}|\boldsymbol{\alpha}) \tag{21}$$

with the distributions on the right-hand side as defined by Eqs. (17)-(20). The product of the prior PDFs $p(\beta)p(\boldsymbol{b})p(\gamma)p(\rho)p(\boldsymbol{\alpha})p(\boldsymbol{T})$ is omitted for convenience, since they are all chosen as broad uniform distributions.

3. Bayesian Inference

For structural damage identification, the damage parameter $\boldsymbol{\theta}$ is of key interest. Therefore, temperature $\boldsymbol{T}$ is treated as a "nuisance" parameter and integrated out to get the posterior distribution of $\boldsymbol{\theta}$

$$\begin{aligned} p\left(\boldsymbol{\theta}|\hat{\boldsymbol{\lambda}}, \hat{\boldsymbol{\psi}}, \hat{\boldsymbol{T}}, \beta, \boldsymbol{b}, \gamma, \rho, \boldsymbol{\alpha}\right) &= \int p\left(\boldsymbol{\theta}, \boldsymbol{T}|\hat{\boldsymbol{\lambda}}, \hat{\boldsymbol{\psi}}, \hat{\boldsymbol{T}}, \beta, \boldsymbol{b}, \gamma, \rho, \boldsymbol{\alpha}\right) d\boldsymbol{T} \\ &= \int p\left(\boldsymbol{\theta}|\, \hat{\boldsymbol{\lambda}}, \hat{\boldsymbol{\psi}}, \boldsymbol{T}, \beta, \boldsymbol{b}, \gamma, \boldsymbol{\alpha}\right) p\left(\boldsymbol{T}|\hat{\boldsymbol{T}}, \rho\right) d\boldsymbol{T} \end{aligned} \tag{22}$$

Under the assumption that the posterior PDF $p\left(\boldsymbol{T}|\hat{\boldsymbol{T}}, \rho\right)$ has a unique maximum at the maximum a posterior (MAP) value $\tilde{\boldsymbol{T}}$, the posterior distribution of $\boldsymbol{\theta}$ can be approximated

as [29, 60]

$$p(\boldsymbol{\theta}|\hat{\boldsymbol{\lambda}},\hat{\boldsymbol{\Psi}},\hat{\boldsymbol{T}},\beta,\boldsymbol{b},\gamma,\rho,\boldsymbol{\alpha}) \approx p(\boldsymbol{\theta}|\,\hat{\boldsymbol{\lambda}},\hat{\boldsymbol{\Psi}},\tilde{\boldsymbol{T}},\beta,\boldsymbol{b},\gamma,\rho,\boldsymbol{\alpha}) \propto p(\hat{\boldsymbol{\lambda}}|\boldsymbol{\theta},\tilde{\boldsymbol{T}},\beta,\boldsymbol{b})p(\hat{\boldsymbol{\Psi}}|\boldsymbol{\theta},\gamma)p(\boldsymbol{\theta}|\boldsymbol{\alpha}) \tag{23}$$

where $\tilde{\boldsymbol{T}} = \arg\max p(\boldsymbol{T}|\hat{\boldsymbol{T}},\rho)$.

As shown in Eq. (23), the posterior PDF of $\boldsymbol{\theta}$ depends on the estimates of the hyper-parameters $\boldsymbol{\delta} = [\beta,\gamma,\boldsymbol{\alpha}]$ and coefficient $\boldsymbol{b}$. Given $\boldsymbol{b}$, the most probable value of $\boldsymbol{\delta}$ can be obtained by maximizing $p(\boldsymbol{\delta}|\hat{\boldsymbol{\lambda}},\hat{\boldsymbol{\Psi}},\tilde{\boldsymbol{T}})$. Assuming that the prior $p(\boldsymbol{\delta})$ are uniformly distributed,

$$p(\boldsymbol{\delta}|\hat{\boldsymbol{\lambda}},\hat{\boldsymbol{\Psi}},\tilde{\boldsymbol{T}}) = \frac{p(\hat{\boldsymbol{\lambda}},\hat{\boldsymbol{\Psi}},\tilde{\boldsymbol{T}}|\boldsymbol{\delta})p(\boldsymbol{\delta})}{p(\hat{\boldsymbol{\lambda}},\hat{\boldsymbol{\Psi}},\tilde{\boldsymbol{T}})} \propto p(\hat{\boldsymbol{\lambda}},\hat{\boldsymbol{\Psi}},\tilde{\boldsymbol{T}}|\boldsymbol{\delta}) \tag{24}$$

Consequently, $\boldsymbol{\delta}$ can be estimated by maximizing the evidence $p(\hat{\boldsymbol{\lambda}},\hat{\boldsymbol{\Psi}},\tilde{\boldsymbol{T}}|\boldsymbol{\delta})$, which can be calculated by integrating over the damage parameter as

$$p(\hat{\boldsymbol{\lambda}},\hat{\boldsymbol{\Psi}},\tilde{\boldsymbol{T}}|\boldsymbol{\delta}) = \int p(\boldsymbol{\theta},\hat{\boldsymbol{\lambda}},\hat{\boldsymbol{\Psi}},\tilde{\boldsymbol{T}}|\boldsymbol{\delta})d\boldsymbol{\theta} = \int p(\hat{\boldsymbol{\lambda}}|\boldsymbol{\theta},\tilde{\boldsymbol{T}},\beta)p(\hat{\boldsymbol{\Psi}}|\boldsymbol{\theta},\gamma)p(\boldsymbol{\theta}|\boldsymbol{\alpha})d\boldsymbol{\theta} \tag{25}$$

However, since the modal data are a nonlinear function of the structural damage parameter, the integral in Eq. (25) cannot be calculated directly.

In this study, the EM algorithm is employed to calculate the damage parameter and hyper-parameters through performing an expectation (E) step and a maximization (M) step iteratively [58, 61, 62]. $\boldsymbol{\theta}$ is regarded as the latent variable and the complete data set is denoted as $(\boldsymbol{\theta},\hat{\boldsymbol{\lambda}},\hat{\boldsymbol{\Psi}},\tilde{\boldsymbol{T}})$. As the direct maximization of $p(\hat{\boldsymbol{\lambda}},\hat{\boldsymbol{\Psi}},\tilde{\boldsymbol{T}}|\boldsymbol{\delta})$ is difficult, the EM algorithm proposes to maximize the expectation of the complete-data natural log likelihood function instead, that is

$$\begin{aligned} E\{\ln p(\boldsymbol{\theta},\hat{\boldsymbol{\lambda}},\hat{\boldsymbol{\Psi}},\tilde{\boldsymbol{T}}|\boldsymbol{\delta})\} &= E\{\ln p(\hat{\boldsymbol{\lambda}}|\boldsymbol{\theta},\tilde{\boldsymbol{T}},\beta) + \ln p(\hat{\boldsymbol{\Psi}}|\boldsymbol{\theta},\gamma) + \ln p(\boldsymbol{\theta}|\boldsymbol{\alpha})\} \\ &= \frac{N_m \cdot N_e}{2}\ln\left(\frac{\beta}{2\pi}\right) - \frac{\beta}{2}E\left\{\sum_{n=1}^{N_s}\sum_{r=1}^{N_m}\left[\frac{\lambda_{r,n}(\boldsymbol{\theta}) + b_r(\tilde{T}_n - T_0) - \hat{\lambda}_{r,n}}{\hat{\lambda}_{r,n}}\right]^2\right\} \end{aligned} \tag{26}$$

$$+\frac{N_p \cdot N_m}{2}\ln\left(\frac{\gamma}{2\pi}\right)-\frac{\gamma}{2}E\left\{\sum_{r=1}^{N_m}\sum_{j=1}^{N_p}\left[\hat{\phi}_{j,r}-\phi_{j,r}(\boldsymbol{\theta})\right]^2\right\}+\frac{N_e}{2}\ln\left(\frac{1}{2\pi}\right)+\frac{1}{2}\sum_{i=1}^{N_e}\ln\alpha_i$$

$$-\frac{1}{2}\sum_{i=1}^{N_e}\alpha_i E(\theta_i^2)$$

Since the complete data set is not available, in the E step, the expectation of the complete data in Eq. (26) is performed with respect to the posterior distribution $p\left(\boldsymbol{\theta}\middle|\hat{\boldsymbol{\lambda}},\hat{\boldsymbol{\psi}},\tilde{\boldsymbol{T}},\boldsymbol{\delta}\right)$ given the current hyper-parameters $\boldsymbol{\delta}^{old}$. In the subsequent M step, the hyper-parameters are updated by maximizing the expectation with respect to β, γ, and $\boldsymbol{\alpha}$, respectively. The hyper-parameters are then obtained by setting the derivatives to zero, such that

$$\beta=\frac{N_m \cdot N_s}{E\left\{\sum_{n=1}^{N_s}\sum_{r=1}^{N_m}\left[\frac{\lambda_{r,n}(\boldsymbol{\theta})+b_r\left(\tilde{T}_n-T_0\right)-\hat{\lambda}_{r,n}}{\hat{\lambda}_{r,n}}\right]^2\right\}} \tag{27}$$

$$\gamma=\frac{N_p \cdot N_m}{E\left\{\sum_{r=1}^{N_m}\sum_{j=1}^{N_p}\left[\hat{\phi}_{j,r}-\phi_{j,r}(\boldsymbol{\theta})\right]^2\right\}} \tag{28}$$

$$\alpha_i=\frac{1}{E(\theta_i^2)} \tag{29}$$

With the obtained hyper-parameters $\boldsymbol{\delta}=\{\beta,\gamma,\boldsymbol{\alpha}\}$, the MAP estimate $\tilde{\boldsymbol{\theta}}$ is calculated by maximising the posterior PDF given by Eq. (23), or equivalently minimising the following objective function

$$J(\boldsymbol{\theta})=\beta\sum_{n=1}^{N_s}\sum_{r=1}^{N_m}\left[\frac{\lambda_{r,n}(\boldsymbol{\theta})+b_r\left(\tilde{T}_n-T_0\right)-\hat{\lambda}_{r,n}}{\hat{\lambda}_{r,n}}\right]^2+\gamma\sum_{r=1}^{N_m}\sum_{j=1}^{N_p}\left[\hat{\phi}_{j,r}-\phi_{j,r}(\boldsymbol{\theta})\right]^2+\sum_{i=1}^{N_e}(\alpha_i\theta_i^2) \tag{30}$$

With the value of $\boldsymbol{\theta}$ fixed at the MAP value, the optimal value of the regression coefficient can be calculated by solving $\partial J(\boldsymbol{\theta})/\partial\boldsymbol{b}=0$, which gives the following equation

$$b_r=\frac{\sum_{n=1}^{N_s}\frac{\left(\tilde{T}_n-T_0\right)\left[\hat{\lambda}_{r,n}-\lambda_{r,n}(\boldsymbol{\theta})\right]}{\hat{\lambda}_{r,n}{}^2}}{\sum_{n=1}^{N_s}\frac{\left(\tilde{T}_n-T_0\right)^2}{\hat{\lambda}_{r,n}{}^2}} \tag{31}$$

Given the MAP value $\widetilde{\boldsymbol{\theta}}$, $\boldsymbol{b}$, and $\boldsymbol{\delta}$, the posterior PDF of $\boldsymbol{T}$ can be expressed as

$$p\left(T\middle|\hat{\boldsymbol{\lambda}},\hat{T},\widetilde{\boldsymbol{\theta}},\beta,\boldsymbol{b},\rho\right) \propto p\left(\hat{\boldsymbol{\lambda}}\middle|\widetilde{\boldsymbol{\theta}},T,\beta,\boldsymbol{b}\right)p\left(\hat{T}\middle|T,\rho\right)$$
$$= \left(\frac{\beta}{2\pi}\right)^{\frac{N_m\cdot N_s}{2}} exp\left\{-\frac{\beta}{2}\sum_{n=1}^{N_s}\sum_{r=1}^{N_m}\left[\frac{\lambda_{r,n}\left(\widetilde{\boldsymbol{\theta}}\right)+b_r(T_n-T_0)-\hat{\lambda}_{r,n}}{\hat{\lambda}_{r,n}}\right]^2\right\} \tag{32}$$
$$\left(\frac{\rho}{2\pi}\right)^{\frac{N_s}{2}} exp\left\{-\frac{\rho}{2}\sum_{n=1}^{N_s}\left(\hat{T}_n-T_n\right)^2\right\}$$

The MAP values of $\boldsymbol{T}$ can be found by minimizing the negative logarithm of the posterior PDF as

$$J(\boldsymbol{T},\gamma)=\beta\sum_{n=1}^{N_s}\sum_{r=1}^{N_m}\left[\frac{\lambda_{r,n}\left(\widetilde{\boldsymbol{\theta}}\right)+b_r(T_n-T_0)-\hat{\lambda}_{r,n}}{\hat{\lambda}_{r,n}}\right]^2-N_s\ln\left(\frac{\rho}{2\pi}\right)+\rho\sum_{n=1}^{N_s}\left(\hat{T}_n-T_n\right)^2 \tag{33}$$

Since $\boldsymbol{T}$ and the associated hyper-parameter ρ are coupled, they are determined through the iterative minimization of the objective function in Eq. (33). The optimal value of $\boldsymbol{T}$ can be obtained by solving $J(\boldsymbol{T},\rho)/\partial T_n=0$, that is

$$T_n=\frac{\rho\hat{T}_n-\beta\sum_{r=1}^{N_m}\frac{b_r}{\hat{\lambda}_{r,n}^{\,2}}\left[\lambda_r\left(\widetilde{\boldsymbol{\theta}}\right)-b_rT_0-\hat{\lambda}_{r,n}\right]}{\beta\sum_{r=1}^{N_m}\left(\frac{b_r}{\hat{\lambda}_{r,n}}\right)^2+\rho} \tag{34}$$

Given $\boldsymbol{T}$, ρ can be obtained by solving $J(\boldsymbol{T},\rho)/\partial\rho=0$, that is

$$\rho=\frac{N_s}{\sum_{n=1}^{N_s}\left(\hat{T}_n-T_n\right)^2} \tag{35}$$

The above formulations can be summarized as the following procedures:

---

1. Initialize $\beta^{(0)}$, $\gamma^{(0)}$, $\alpha_i^{(0)}$ $(i=1,2,\dots,N)$, $\boldsymbol{b}^{(0)}$, $\rho^{(0)}$, and $T_n^{(0)}$;

2. At the *j*th iteration,

   (1) Given $\beta^{(j-1)}$, $\gamma^{(j-1)}$, $\boldsymbol{\alpha}^{(j-1)}$, $\boldsymbol{b}^{(0)}$, and $T^{(j-1)}$:

   Compute the MAP estimate of $\widetilde{\boldsymbol{\theta}}^{(j)}$ through minimising $J(\boldsymbol{\theta})$ in Eq. (30);

   Update $\beta^{(j)}$, $\gamma^{(j)}$, and $\boldsymbol{\alpha}^{(j)}$ using Eqs. (27), (28), and (29);

Update $\boldsymbol{b}^{(j)}$ using Eq. (31)

(2) Given $\widetilde{\boldsymbol{\theta}}^{(j)}$, $\beta^{(j)}$, $\boldsymbol{b}^{(j)}$, and $\rho^{(j-1)}$:

Update $T^{(j)}$ using Eq. (34);

Update $\rho^{(j)}$ using Eq. (35).

3. Repeat Step 2 until the convergence criterion is satisfied:

$$\left\| \widetilde{\boldsymbol{\theta}}^{(j)} - \widetilde{\boldsymbol{\theta}}^{(j-1)} \right\|_2 / \left\| \widetilde{\boldsymbol{\theta}}^{(j)} \right\|_2 \leq Tol$$

4. An Experimental Example

4.1 Description of the experiment

The experimental two-storey steel frame presented in Bao et al. [53] is used here to demonstrate the effectiveness of the proposed technique. The geometric dimensions of the frame are shown in Fig. 1. The mass density and Young's modulus are estimated as 7.67×10^3 kg/m^3 and 2.0×10^{11} N/m^2, respectively.

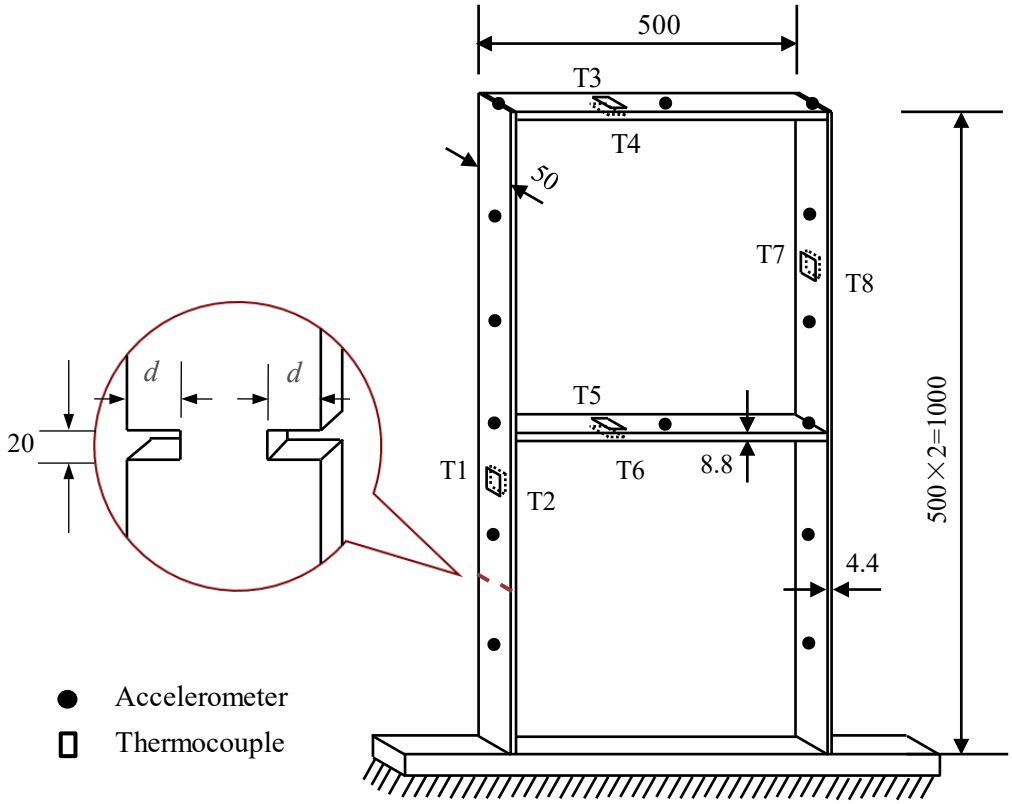

Fig. 1. Geometric configuration of the frame structure (unit: mm)

The temperature of the frame was measured using 8 thermocouples, denoted as T1–T8 in Fig. 1. 12 accelerometers were equidistantly mounted on the columns and 2 at the midpoints of the beams to measure the acceleration signals. An instrumented hammer was used to excite the experimental model.

The modal testing was first conducted on the intact frame with the sampling frequency of 2048 Hz. The vibration tests were performed every 20 minutes from morning to afternoon, resulting in 28 sets ($N_s = 28$) of vibration data throughout the day. After each test, the natural frequencies and mode shapes were extracted using the modal analysis. The temperature of the frame was also measured during the test.

Damage was then subsequently introduced to the frame model as shown in Fig. 1. The saw cut has the length of 20 mm and depths of d = 5, 10, and 15 mm corresponding to three damage scenarios (DSs). The moment of inertia of the cut sections were then reduced by 20%,

40%, and 60%. For each DS, the aforementioned modal testing was repeated from morning to afternoon and temperature was also recorded.

The first five natural frequencies and modal assurance criterion (MAC) ($N_m = 5,\ N_p = 14$) of the frame model in the undamaged and three damaged states are compared in Table 1. The frequencies and MAC displayed are the average values extracted from the total 28 sets of vibration data. The variations in the natural frequencies caused by damage are very small with a maximum average change of 0.65%. The temperature data of the frame in the undamaged and damaged states are shown in Fig. 2, in which the mean value of the eight thermocouples was plotted. During the test period, the temperature varied between 29.5℃ and 52.2℃.

Table 1 Frequencies and MAC of the frame in the undamaged and damaged states

Mode	Undamaged	DS1: d=5 mm		DS2: d=10 mm		DS3: d=15 mm	
No.	Freq. (Hz)	Freq. (Hz)	MAC	Freq. (Hz)	MAC	Freq. (Hz)	MAC
1	6.20	6.19 (–0.19)	99.99	6.17 (–0.43)	99.79	6.19 (–0.13)	99.78
2	17.57	17.49 (–0.49)	99.82	17.48 (–0.52)	99.80	17.45 (–0.72)	99.80
3	61.07	60.97 (–0.17)	99.72	60.83 (–0.39)	99.98	60.74 (–0.55)	99.98
4	77.01	76.97 (–0.05)	99.18	76.65 (–0.47)	98.56	76.32 (–0.89)	98.56
5	80.83	80.73 (–0.13)	99.16	80.16 (–0.83)	86.95	80.05 (–0.97)	86.93
Average		(–0.21)	99.56	(–0.53)	98.81	(–0.65)	96.09

Values in parentheses are the frequency change ratios (%) between the damaged and undamaged states.

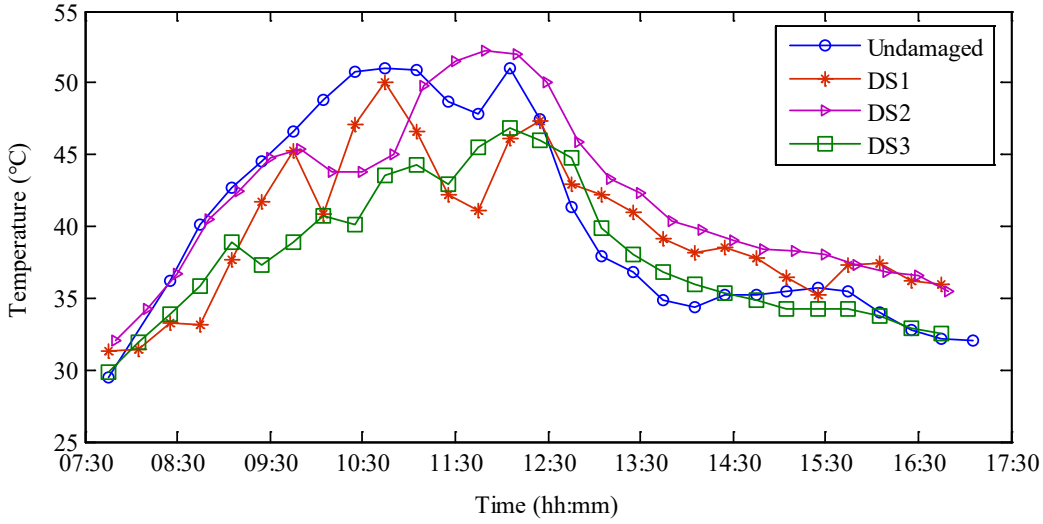

Fig. 2. Measured temperature of the frame in different states

The relation between the natural frequencies and temperature in each state is shown in Fig. 3. In general, all five natural frequencies decrease with the increase of temperature and damage severity. However, the temperature may cause more significant change in the frequencies than damage does. For example, in Fig. 3(c), the third natural frequency of the frame in DS1 at 32℃ is larger than that in the undamaged state at 50℃. Other modes and other damage states have similar phenomenon. Therefore, the temperature effects should be considered in order to achieve an accurate damage identification. The first five mode shapes do not show the correlation with temperature, as observed in other studies [38]. The details are not shown here for brevity and can be referred to Reference [53].

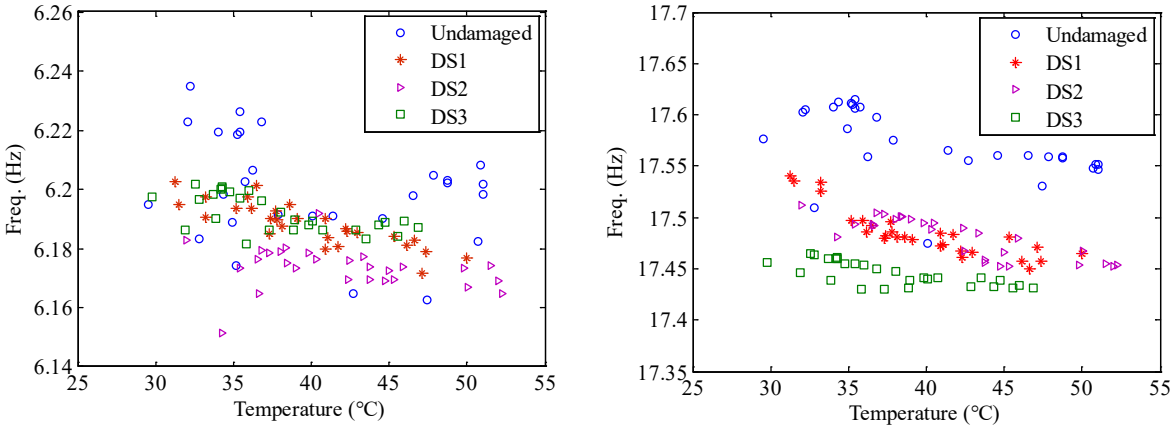

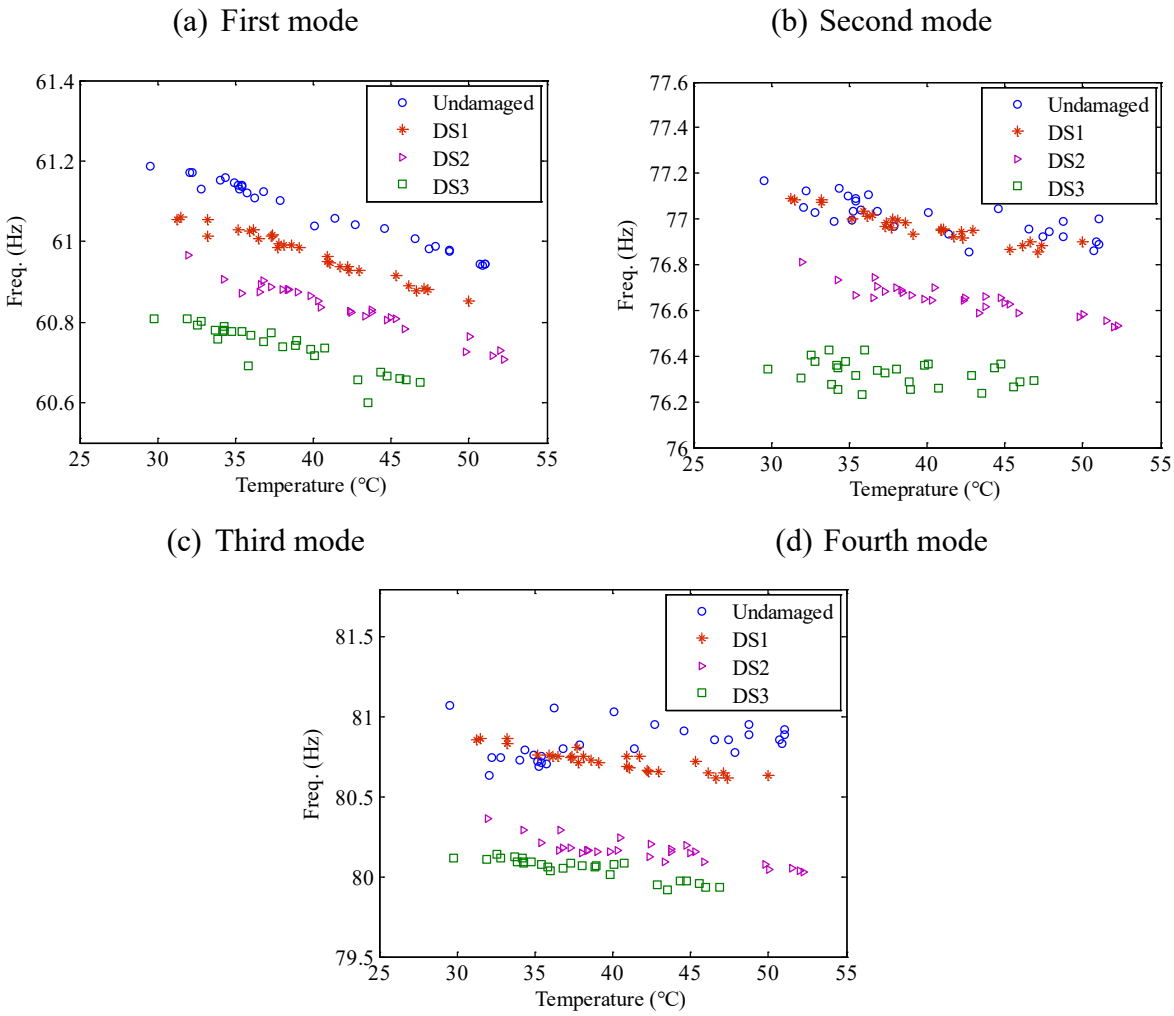

Fig. 3. Relation of frequencies to temperature

The frame is modelled using 20 Euler–Bernoulli beam elements as presented in Bao et al. [53]. Each column is equidistantly divided into 6 elements and each beam into 4 elements. The saw cut is located at element 2. The equivalent stiffness reductions of the damaged element for the three DSs are about 3%, 7%, and 15%, respectively [53].

4.2 Damage detection

The first five natural frequencies and mode shapes are used for damage identification. The hyper-parameters need to be initialized first. The uncertainty of the modal data can be

quantified by Bayesian modal identification [63] or Monte Carlo analysis [64]. In this study, they are estimated empirically. In practical vibration tests, natural frequencies may typically contain 1% noise and are generally measured more accurately than mode shapes [65]. In this regard, the uncertainty levels of 1% and 5% are adopted for natural frequencies and mode shapes, respectively. Therefore, the initial values $\beta^{(0)}=1/(0.01)^2=1\times10^4$ and $\gamma^{(0)}=1/(0.05)^2=400$. The uncertainty level of the damage parameter is assumed as 10% of the exact value, namely $\alpha_i^{(0)}=1/(10\%)^2=100$ (i=1, 2,…, N). The uncertain level of 0.1% is assigned to temperature, that is $\rho^{(0)}=1/(0.001)^2=1\times10^6$. The initial damage parameter is assumed as $\boldsymbol{\theta}^{(0)}=\{0,\ldots,0\}^{\mathrm{T}}$, indicating that no damage is present. According to Eq. (23), the initial values of temperature are chosen as the measured ones $T_n^{(0)}=\hat{T}_n$ $(n=1,2,\ldots,N_s)$. The regression coefficient is initialized as the one obtained using least-squares fitting. The reference temperature is set to 40℃ as in Bao et al. [53].

For the current experimental frame, 28 sets of measured modal data are available, i.e., $\boldsymbol{\mathcal{D}}_Y=[\hat{\boldsymbol{\lambda}}_n,\hat{\boldsymbol{\psi}}_n]$ $(n=1,2,\ldots,28)$. Within EM, each set of modal data results in one set of MAP values of the damage parameter, from which the expectations are calculated according to Eqs. (27)-(29). For DS1, the mean of the MAP values of $\boldsymbol{\theta}$ in each iteration are shown in Fig. 4. In the first iteration, several elements have nonzero SRFs. After 4 iterations only, the actual damage at element No. 2, although very slight (–3%), is successfully located and quantified. In DS2 and DS3, the convergences are achieved after five and nine iterations, respectively. The iterative identification results are shown in Figs. 5 and 6. For brevity, only the results in the first two and the last two iterations are shown. Upon convergence, the actual damaged element is correctly located and quantified.

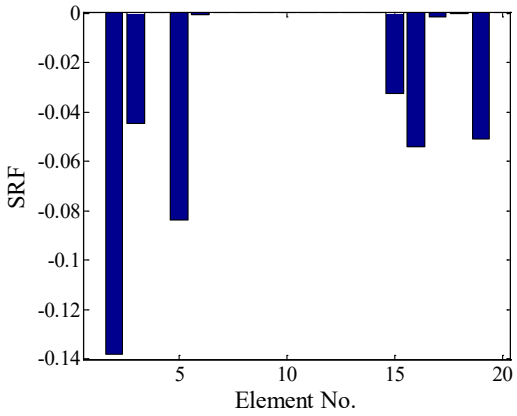

(a) Iteration No. 1

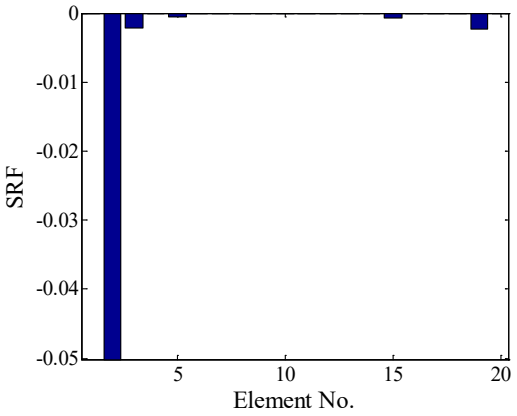

(b) Iteration No. 2

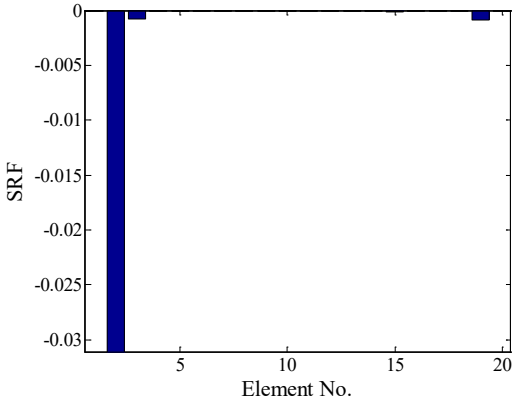

(c) Iteration No. 3

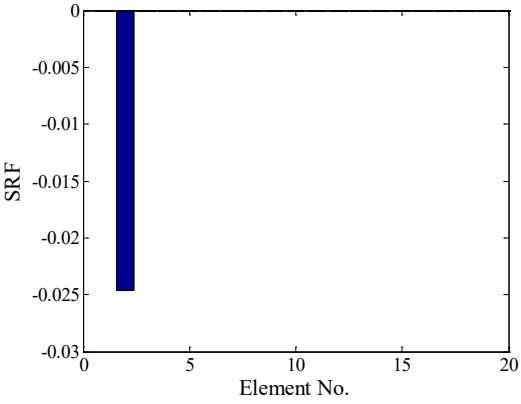

(d) Iteration No. 4

Fig. 4. Damage identification results in DS1 during the iterative process

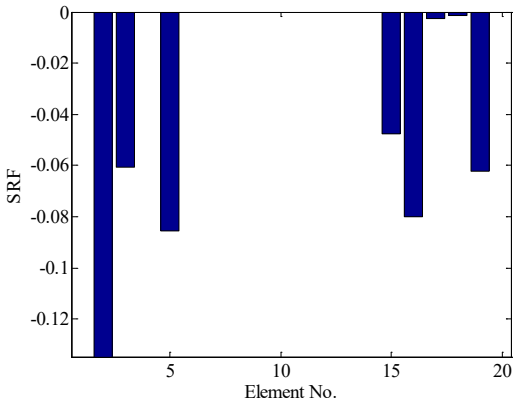

(a) Iteration No. 1

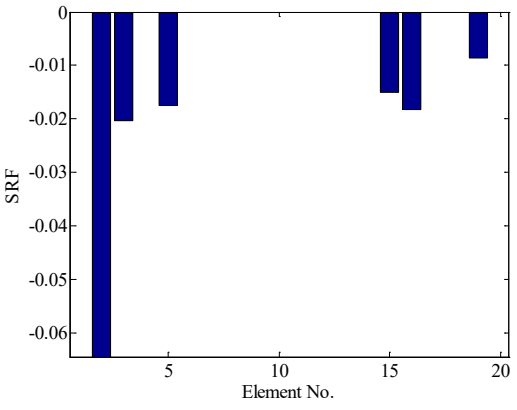

(b) Iteration No. 2

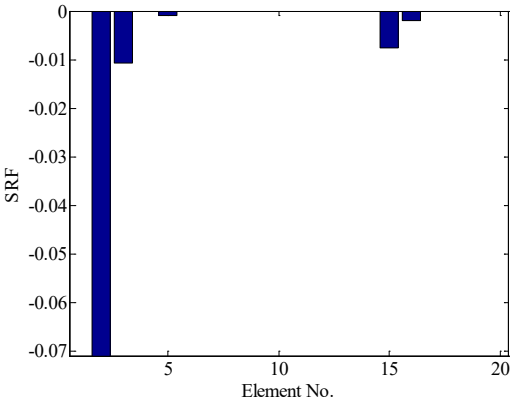

(c) Iteration No. 4

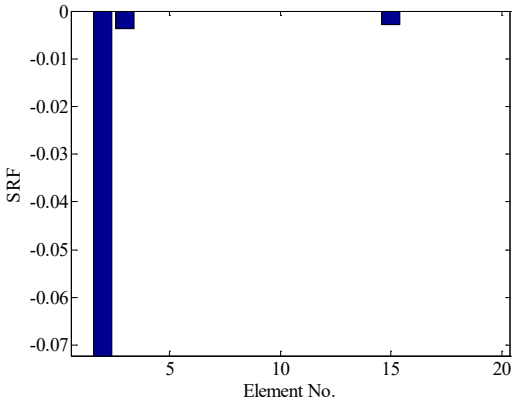

(d) Iteration No. 5

Fig. 5. Damage identification results in DS2 during the iterative process

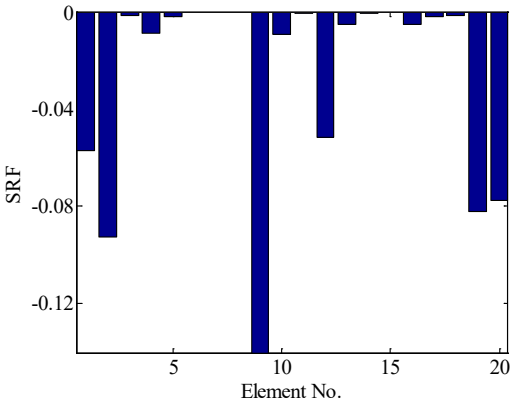

(a) Iteration No. 1

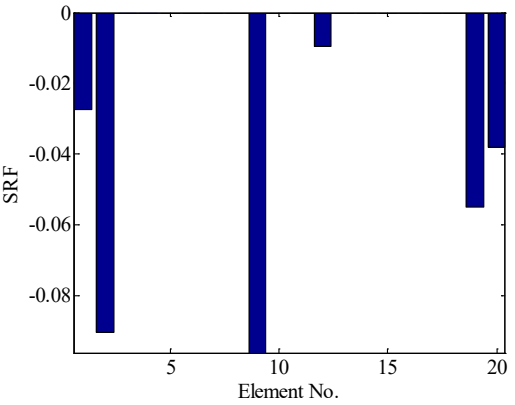

(b) Iteration No. 2

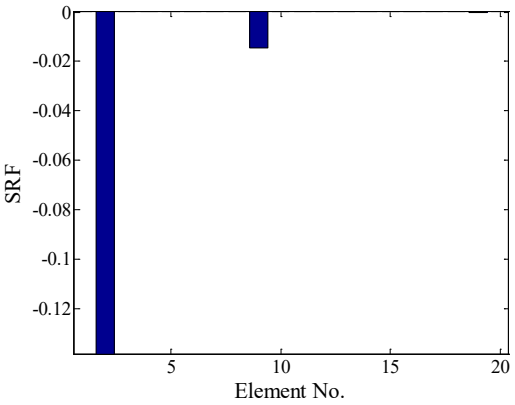

(c) Iteration No. 8

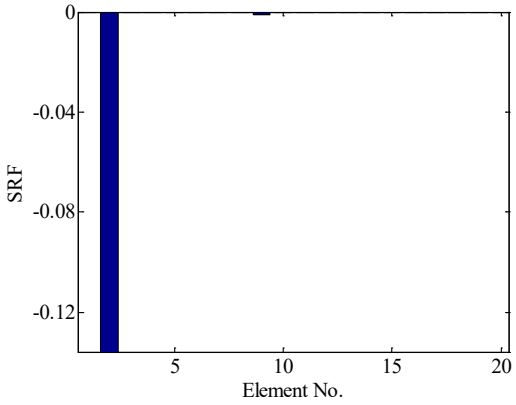

(d) Iteration No. 9

Fig. 6. Damage identification results in DS3 during the iterative process

During the iteration process, the hyper-parameters also change continuously. α_2 corresponds to the damaged element while α_{19} to the undamaged one. α_2 and α_{19} in the three damage scenarios are shown in Fig. 7. As the iteration proceeds, α_2 converges after a few iterations while α_{19} increases quickly to a sizeable number (a logarithmic coordinate is used). This phenomenon explains the sparse mechanism of the SBL. Within SBL, each damage parameter is assigned an individual hyper-parameter α_i. The hyper-parameters of the undamaged parameters increase significantly larger than that of the damaged ones. Minimisation of the objective function in Eq. (30) enforces the undamaged θ_i to be close to zero, thereby achieving sparsity of the damage parameter.

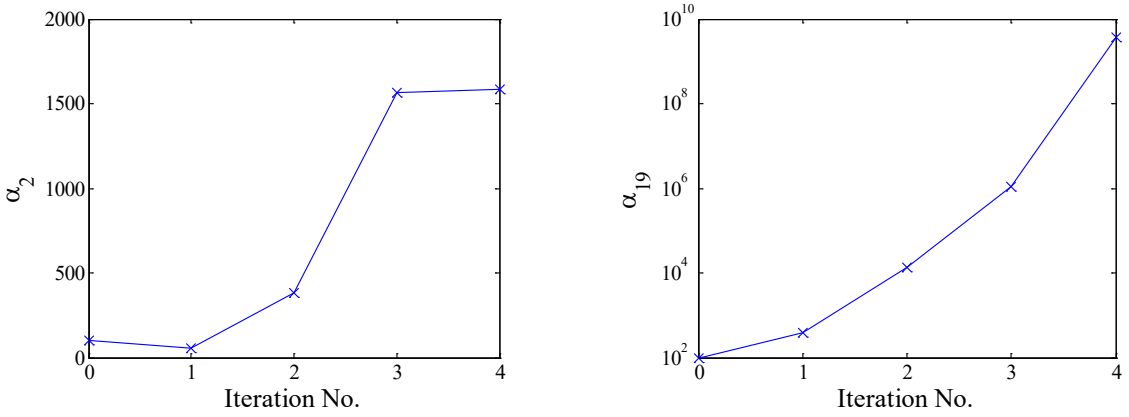

(a) DS1

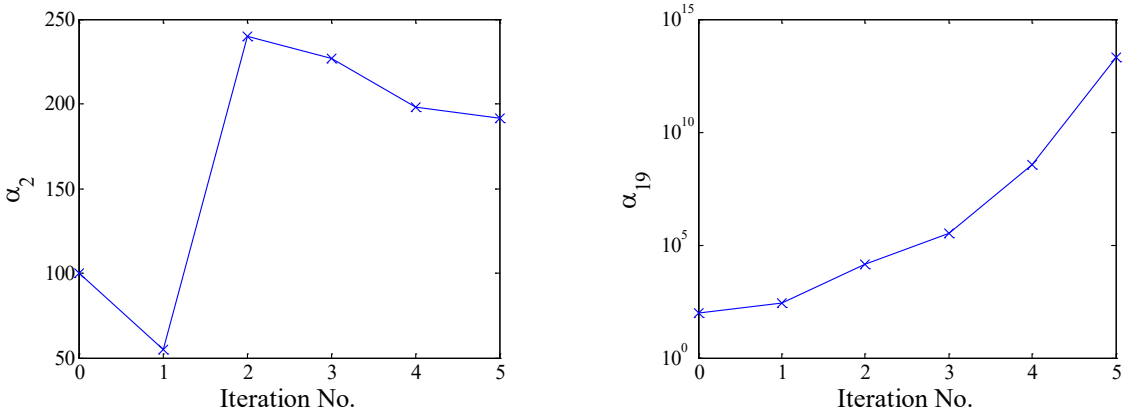

(b) DS2

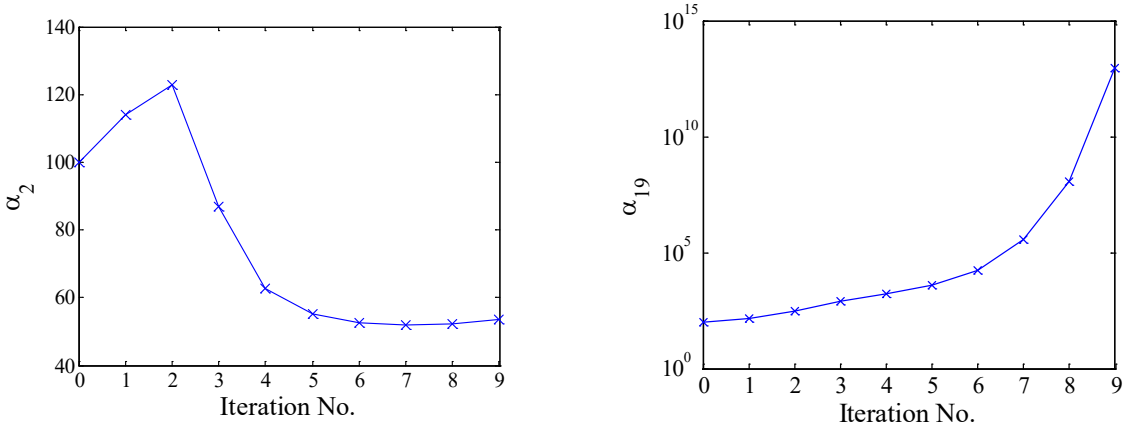

(c) DS3

Fig. 7. Variation of hyper-parameters (α_i) during the iterative process

4.3 Results Comparison

For the comparison purpose, damage identification is also conducted without considering varying temperature. In the case, the frequencies measured at different temperature are averaged and then used for damage detection, which is similar to the study in Hou et al. [58]. The results with and without considering temperature effects are compared in Fig. 8. For all 3 DSs, the damaged element is determined correctly, and the identified SRFs are very close to the true values when the temperature effects are taken into account. However, if the frequency change caused by the temperature variation is not considered, although the true damage is located, the identified damage severities are far from the actual values.

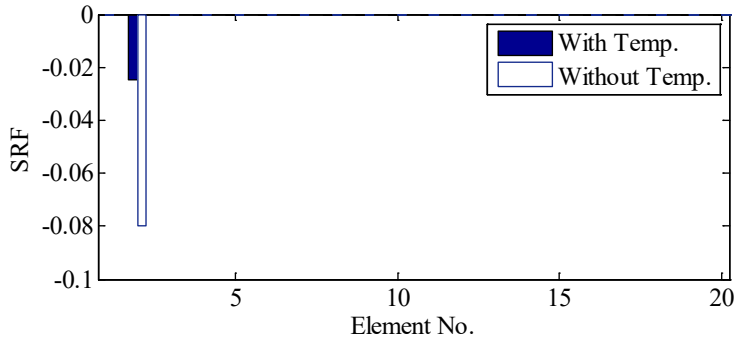

(a) DS1: SRF_2= –0.03

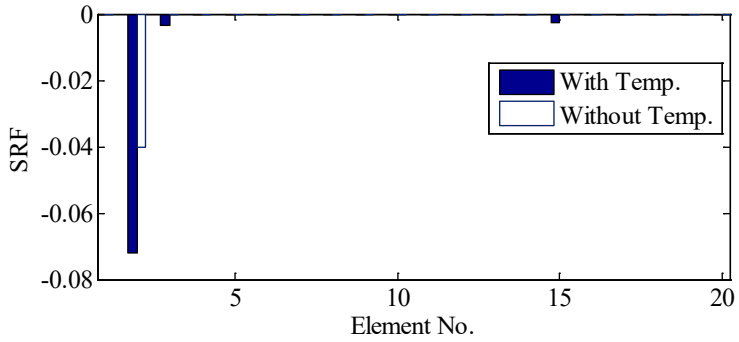

(b) DS2: $SRF_2 = -0.07$

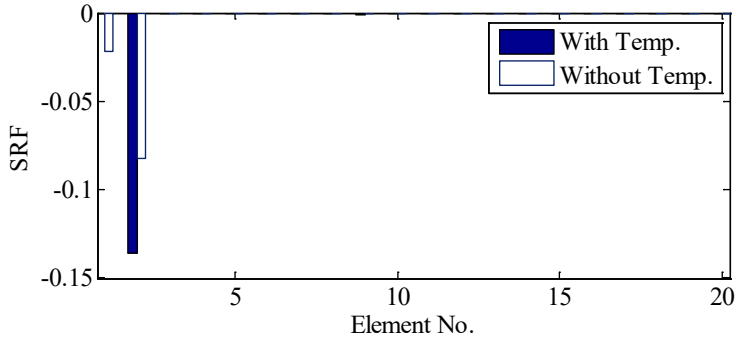

(c) DS3: $SRF_2 = -0.15$

Fig. 8. Damage identification results with and without considering temperature effects

5. Conclusions and Discussions

An SBL technique for damage detection under varying temperature conditions is developed in this study. A new Bayesian model updating framework is proposed, which simultaneously considers the uncertainties in the measured modal data and FE model and varying temperature. The correlation between temperature and natural frequencies is incorporated into the SBL framework. The damage parameter is identified through the iterative EM technique.

Compared with the technique proposed in Bao et al. [53] which can only determine the damage location, the presented method cannot only identify damage location but also quantify damage severity. The experimental example demonstrates that the proposed method is effective in locating and quantifying structural damage, even when the variation of the modal data caused by damage is very small. The accuracy of the damage detection results is

improved significantly, compared with those without considering the temperature effects.

A linear model between the natural frequencies and temperature is used in this study. The proposed Bayesian framework is still feasible when a high-order polynomial model is employed. In this case, the most plausible temperature model, which is able to successfully characterize the temperature effects on the natural frequencies, can be determined based on the Bayesian model class selection [63].

Acknowledgements

The work described in this paper was substantially supported by the funding for Projects of Strategic Importance of The Hong Kong Polytechnic University (Project Code: 1-ZE1F) and the funding for the Guangdong Provincial Key R&D program (Project No.: 2019B111106001).

References

1. S.W. Doebling, C.R. Farrar, M.B. Prime, D.W. Shevitz, Damage identification and health monitoring of structural and mechanical systems from changes in their vibration characteristics: a literature review, Los Alamos National Laboratory Report LA–13070–MS, USA, 1996.

2. H. Sohn, C.R. Farrar, F.M. Hemez, D.D. Shunk, S.W. Stinemates, B.R. Nadler, J.J. Czarnecki, A review of structural health monitoring literature: 1996–2001, Los Alamos National Laboratory report LA–13976–MS, USA, 2003.

3. E.P. Carden, P. Fanning, Vibration based condition monitoring: a review, Struct. Health Monitor. 3 (2004) 355–377.

4. W. Fan, P.Z. Qiao, Vibration-based damage identification methods: a review and comparative study, Struct. Health Monitor. 10 (2011) 83–111.

5. X. Kong, C.S. Cai, J.X. Hu, The state-of-the-art on framework of vibration-based Sstructural damage identification for decision making, Appl. Sci. 7 (2017) 497.

6. O.S. Salawu, Detection of structural damage through changes in frequency: a review, Eng. Struct. 19 (1997) 718–723.

7. J.H. Zhao, L. Zhang, Structural damage identification based on the modal data change, Int. J. Eng. Man. 4 (2012) 59–66.

8. M.K. Yoon, D. Heider, J.W. Gillespie Jr., C.P. Ratcliffe, R.M. Crane, Local damage detection with the global fitting method using operating deflection shape data, J. Nondestruct. Eval. 29 (2010) 25–37.

9. D.M. Feng, M.Q. Feng, Output-only damage detection using vehicle-induced displacement response and mode shape curvature index, Struct. Control Health Monit. 23 (2016) 1088–1107.

10. Y.Q. Bao, H. Li, J.P. Ou, Emerging data technology in structural health monitoring: compressive sensing technology, J. Civ. Struct. Health Monit. 4 (2014) 77–90.

11. H. Aied, A. Gonzáleza, D. Cantero, Identification of sudden stiffness changes in the acceleration response of a bridge to moving loads using ensemble empirical mode decomposition, Mech. Syst. Signal Process. 66 (2016) 314–338.

12. R. Ghiasi, P. Torkzadeh, M. Noori, A machine-learning approach for structural damage detection using least square support vector machine based on a new combinational kernel function, Struct. Health Monit. 15 (2016) 302–316.

13. Y. Huang, C. Shao, B. Wu, J.L. Beck, H. Li, State-of-the-art review on Bayesian inference in structural system identification and damage assessment, Adv. in Struct. Eng 22 (6) (2019) 1329–1351.

14. M. Gordan, H.A. Razak, Z. Ismail, K. Ghaedi, Recent developments in damage identification of structures using data mining, Lat. Am. J. Solids Stru. 14 (13) (2017) 2373–2401.

15. Y.Q. Bao, Z.C. Chen, S.Y. Wei, Y. Xu, Z.Y. Tang, H. Li, The state of the art of data science and engineering in structural health monitoring, Engineering 5 (2019) 234–242.

16. Y. Yang, S. Nagarajaiah, Structural damage identification via a combination of blind feature extraction and sparse representation classification, Mech. Syst. Signal Process. 45 (2014) 1–23.

17. X.Q. Zhou, Y. Xia, S. Weng, L_1 regularization approach to structural damage detection using frequency data, Struct. Health Monitor. 14 (2015) 571–582.

18. Y.Q. Bao, H. Li, Z.C. Chen, F.J. Zhang, A.X. Guo, Sparse l_1 optimization-based identification approach for the distribution of moving heavy vehicle loads on cable-stayed bridges, Struct. Control Health Monit. 23 (2016) 144–155.

19. R.R. Hou, Y. Xia, X.Q. Zhou, Structural damage detection based on l_1 regularization using natural frequencies and mode shapes, Struct. Control Health Monit. 25 (2018) e2107.

20. C.B. Chen, L. Yu, A hybrid ant lion optimizer with improved Nelder–Mead algorithm for structural damage detection by improving weighted trace lasso regularization, Adv. in Struct. Eng. 23 (2019) 468–484.

21. Z.H. Ding, J. Li, H. Hao, Structural damage identification using improved Jaya algorithm based on sparse regularization and Bayesian inference, Mech. Syst. Signal Process. 132 (2019) 211–231.

22. Y. Huang, C Shao, B. Wu, J.L. Beck, H. Li, State-of-the-art review on Bayesian inference in structural system identification and damage assessment, Adv. in Struct. Eng. 22 (2019) 1329–1351.

23. R. Hajrya, N. Mechbal, Principal component analysis and perturbation theory–based robust damage detection of multifunctional aircraft structure, Struct. Health Monit. 12 (2013) 263–277.

24. S. Arangio, J.L. Beck, Bayesian neural networks for bridge integrity assessment, Struct.

Control Health Monit. 19 (2012) 3–21.

25. E. Simoen, G. De Roeck, G. Lombaert, Dealing with uncertainty in model updating for damage assessment: a review, Mech. Syst. Signal Process. 56 (2015) 123–149.

26. I. Yeo, S. Shin, H.S. Lee, S.P. Chang, Statistical damage assessment of framed structures from static responses, J. Eng. Mech. 126 (2000) 414–421.

27. M. Gul, F.N. Catbas, Statistical pattern recognition for Structural Health Monitoring using time series modeling: theory and experimental verifications, Mech. Syst. Signal Process. 23 (2009) 2192–2204.

28. H. Sohn, K.H. Law, A Bayesian probabilistic approach for structure damage detection, Earthq. Eng. Struct. Dyn. 26 (1997) 1259–1281.

29. J.L. Beck, L.S. Katafygiotis, Updating models and their uncertainties. I: Bayesian statistical framework, J. Eng. Mech. 124 (1998) 455–461.

30. M.W. Vanik, J.L. Beck, S.K. Au, Bayesian probabilistic approach to structural health monitoring, J. Eng. Mech. 126 (2000) 738–745.

31. J. Ching, J.L. Beck, Bayesian analysis of the phase II IASC–ASCE structural health monitoring experimental benchmark data, J. Eng. Mech. 130 (2004) 1233–1244.

32. P.M. Williams, Bayesian regularization and pruning using a Laplace prior, Neural Comput. 7 (1995) 117–143.

33. R.D. Adams, P. Cawley, C.J. Pye, B.J. Stone, A vibration technique for non-destructively assessing the integrity of structures, J. Mech. Eng. 20 (1978) 93–100.

34. C.R. Farrar, P.J. Cornwell, S.W. Doebling, M.B. Prime, Structural health monitoring studies of the Alamosa Canyon and I-40 bridges, Los Alamos National Laboratory Report LA-13635-MS, USA, 2000.

35. H. Sohn, Effects of environmental and operational variability on structural health monitoring, Philos. Trans. R. Soc. A 365 (2007) 539–560.

36. Z.D. Xu, Z.S. Wu, Simulation of the Effect of Temperature Variation on Damage Detection in a Long-span Cable-stayed Bridge, Struct. Health Monit. 6 (2007) 177–189.

37. H. Li, S.L. Li, J.P. Ou, H.W. Li, Modal identification of bridges under varying environmental conditions: Temperature and wind effects, Struct. Control Health Monit. 17 (2010) 499–512.

38. Y. Xia, H. Hao, G. Zanardo, A. Deeks, Long term vibration monitoring of an RC slab: temperature and humidity effect, Eng. Struct. 28 (2006) 441–452.

39. H.F. Zhou, Y.Q. Ni, J.M. Ko, Eliminating temperature effect in Vibration-Based structural damage detection, J. Eng. Mech. 137 (2011) 785–796.

40. B. Peeters, G. De Roeck, One-year monitoring of the Z24–Bridge: Environmental effects versus damage events, Earthq. Eng. Struct. Dyn. 30 (2011) 149–171.

41. C.Y. Liu, J.T. DeWolf, Effect of Temperature on Modal Variability of a Curved Concrete Bridge under Ambient Loads, J. Struct. Eng. 133 (2007) 1742–1751.

42. L. Faravelli, F. Ubertini, C. Fuggini, System identification of a super high-rise building via a stochastic subspace approach, Smart Struct. Syst. **7** (2011) 133–152.

43. H.Q. Mu, K.V. Yuen, Modal frequency-environmental condition relation development using long-term structural health monitoring measurement: Uncertainty quantification, sparse feature selection and multivariate prediction, Meas. 130 (2018) 384–397.

44. H. Sohn, M. Dzwonczyk, E. Straser, A. Kiremidjian, K. Law, T. Meng T, An experimental study of temperature effect on modal parameters of the Alamosa canyon bridge, Earthq. Eng. Struct. Dyn. 28 (1999) 878–897.

45. A.M. Yan, G. Kerschen, P. De Boe, J.C. Golinval, Structural damage diagnosis under changing environmental conditions – Part 1: linear analysis, Mech. Syst. Signal Process. 19 (2005) 847–864.

46. D.F. Giraldo, S.J. Dyke, J.M. Caicedo, Damage detection accommodating varying environmental conditions, Struct. Health Monit. 5 (2006) 155–172.

47. A. Deraemaeker, E. Reynders, G. De Roeck, J. Kullaa, Vibration-based structural health monitoring using output–only measurements under changing environment, Mech. Syst. Signal Process. 22 (2008) 34–56.

48. J.D. Hios, S.D. Fassois, A global statistical model based approach for vibration response–only damage detection under various temperatures: A proof-of-concept study, Mech. Syst. Signal Process. 49 (2014) 77–94.

49. Y. Shokrani, V.K. Dertimanis, E.N. Chatzi, M.N. Savoia, On the use of mode shape curvatures for damage localization under varying environmental conditions, Struct. Control Health Monit. 25 (2018) e2132.

50. M. Fallahian, F. Khoshnoudian, V. Meruane, Ensemble classification method for structural damage assessment under varying temperature, Struct. Health Monit. 17 (2018)

747–762.

51. K. Erazo, D. Sen, S. Nagarajaiah, L.M. Sun, Vibration-based structural health monitoring under changing environmental conditions using Kalman filtering, Mech. Syst. Signal Process. 117 (2019) 1–15.

52. E. Balmes, M. Basseville, F. Bourquin, L. Mevel, H. Nasser, F. Treyssede, Merging sensor data from multiple temperature scenarios for vibration monitoring of civil structures, Struct. Health Monit. **7** (2008) 129–142.

53. Y.Q. Bao, Y. Xia, H. Li, Y.L. Xu, P. Zhang, Data fusion-based structural damage detection under varying temperature conditions, Int. J. Struct. Stab. Dyn. 12 (2012) 1–27.

54. M.E. Tipping, Sparse Bayesian learning and the relevance vector machine, J. Mach. Learn. Res. 1 (2001) 211–244.

55. Y. Huang, J.L. Beck, H. Li, Hierarchical sparse Bayesian learning for structural damage detection: theory, computation and application, Struct. Saf. 64 (2017) 37–53.

56. Y. Huang, H. Li, S. Wu, Y.C. Yang, Fractal dimension based damage identification incorporating multi-task sparse Bayesian learning, Smart Mate. Struct. 27 (7) (2018) 075020.

57. I. Daubechies, R. DeVore, M. Fornasier, C.S. Güntürk, Iteratively reweighted least squares minimization for sparse recovery, Commun. Pur. Appl. Math. 63 (2010) 1–38.

58. R.R. Hou, Y. Xia, X.Q. Zhou, Y. Huang, Sparse Bayesian learning for structural damage detection using expectation–maximization technique, Struct. Control Health Monit. 26 (2019) e2343.

59. H.Q. Mu, K.V. Yuen, Ground motion prediction equation development by heterogeneous Bayesian learning, Comput-Aided Civ. Inf. 31 (2016) 761–776.

60. Y. Huang, J.L. Beck, Hierarchical sparse Bayesian learning for structural health monitoring with incomplete modal data, Int. J. Uncertain. Quan. 5 (2) (2015) 139–169.

61. A.P. Dempster, N. Laird, D. Rubin, Maximum likelihood for incomplete data via the EM algorithm, J. Royal Stat. Soc. Ser. B Methodol. 39 (1977) 1–38.

62. C.M. Bishop. Pattern Recognition and Machine Learning, Springer, Berlin, 2006.

63. K.V. Yuen, S.C. Kuok, Modeling of environmental influence in structural health assessment for reinforced concrete buildings, Earthq. Eng. Eng. Vib. 9 (2010) 295–306.

64. S.W. Doebing, C.R. Farrar, R.S. Goodman, Effects of measurement statistics on the detection of damage in the Alamosa Canyon Bridge, Proc. of the 15th IMAC, Orlando, USA, February 3–6, 1997, 919–929.

65. J.E. Mottershead, M.I. Friswell, Model updating in structural dynamics: a survey, J. Sound Vib. 167 (1993) 347–375.